RSC Advances

COMMUNICATION

View Article Online
View Journal | View Issue

Cite this: *RSC Adv.*, 2015, **5**, 3196

Received 2nd October 2014
Accepted 2nd December 2014

DOI: 10.1039/c4ra14392b

www.rsc.org/advances

Electroless deposition of iridium oxide nanoparticles promoted by condensation of $[Ir(OH)_6]^{2-}$ on an anodized Au surface: application to electrocatalysis of the oxygen evolution reaction†

P. Esakki Karthik,[a] K. Alagar Raja,[a] S. Senthil Kumar,[a] K. L. N. Phani,*[a] Yuping Liu,[b] Si-Xuan Guo,[b] Jie Zhang[b] and Alan M. Bond*[b]

The high reactivity of anodized gold for the condensation of $[Ir(OH)_6]^{2-}$ provides a simple procedure for the electroless deposition of catalytically active IrO_x nanoparticles supported on a gold electrode (IrO_x/Au). With a very low overpotential (η) of only about 370 mV (0.1 M NaOH) required to give a current density of 10 mA cm^{-2}, an average value for a turn over frequency ($TOF_{1.56V}$) of 6.2 s^{-1}, and high stability under long term catalytic turn-over, the IrO_x/Au composite provides the *simplest method yet developed* for highly efficient iridium oxide-based electrocatalysis of the water oxidation reaction.

There is a growing interest in oxygen electrochemistry as conversion reactions between H_2O and O_2 play an important role in renewable energy technologies based on splitting of water into H_2 and O_2. One of the main requirements for oxide-based electrocatalysts used for the oxygen evolution reaction (OER), and used as the anode in water splitting, is the stabilization of a high metal oxidation state in the oxide catalyst.[1] IrO_x continues to be a benchmark oxide catalyst.[2] The electrochemical characteristics of IrO_x are shown to be strongly dependent on the method of film preparation[2] with the catalytically relevant properties being established by *in situ* APXPS[3] and XANES[4,5] measurements.

Electrodeposition provides one of the easiest ways to immobilize metals or their oxides. However, iridium metal electrodeposition is restricted by the fact that to date it has required use of surfaces that are covered by surface-adsorbed hydrogen atoms that reduce Ir^{3+}. Hence, surfaces devoid of adsorbed surface hydrogen atoms such as carbon and gold require alternative indirect methods of deposition. In this context, new chemistries have been developed that facilitate the electroless deposition of IrO_x. Important examples include the deposition of IrO_x nanoparticles on glassy carbon electrodes using controlled potential electro-flocculation from pH $\sim$ 13 nanoparticle solutions[6] and electrogeneration of IrO_x nanoparticles for use as redox catalysts.[7] However, the poor stability of hydrous IrO_x films, especially when used in alkaline conditions, limit their utility[8] and leads to complications in the implementation of OER. The method reported recently by Zhao *et al.*[9] addresses this issue by performing anodic deposition of colloidal IrO_x thin films onto gold from hexahydroxyiridate(IV), $[Ir(OH)_6]^{2-}$, solutions at high anodic potentials. However, in addition to gold oxidation during the anodic deposition, oxygen gas evolution also occurs, leading to destabilization of the IrO_x nanoparticle film. In the present work, we now take advantage of the unique reactivity of anodized gold to develop a new method for the electroless deposition of IrO_x films that avoids mechanical disturbance due to gas bubble formation during the course of film deposition and which is also less energy-consuming.

Anodized gold has been employed to form nanoporous gold[10] for use in sensor applications[11] and to construct high surface area materials.[12] For the first time, we now make use of the high open-circuit potential of the anodized gold to spontaneously form films of IrO_x on a gold substrate which is acknowledged as an ideal support for OER catalysts.[13] The gold surface is anodized in 0.5 M H_2SO_4 at 2.68 V *vs.* RHE for a period of 100 seconds to give the current–time data shown in Fig. 1A. Consistent with our hypothesis, cyclic voltammograms of the anodized gold surface show increased current magnitudes resulting from enhancement in the electrochemical surface area (Fig. 1B). The orange film formed on the surface indicates gold oxidation (Fig. S1†). Electrochemical reduction of the anodized gold electrode yields morphological features consistent with the formation of nanoporous gold, as reported by Nishio and Masuda.[10] In an attempt to establish the form of Au in the orange colored film, reference was made to the Pourbaix diagram[14,15] which suggests the film is based on hydrated $Au(OH)_3$.

[a]*Nanoscale Electrocatalysis Group, Electrodics & Electrocatalysis Division, CSIR-Central Electrochemical Research Institute, Karaikudi, 630006, India. E-mail: klnphani@cecri.res.in; klnp56.kp@gmail.com*

[b]*School of Chemistry, Monash University, Clayton, VIC 3800, Australia. E-mail: alan.bond@monash.edu*

† Electronic supplementary information (ESI) available: Experimental details, electrochemical characterization and details of TOF calculation. See DOI: 10.1039/c4ra14392b

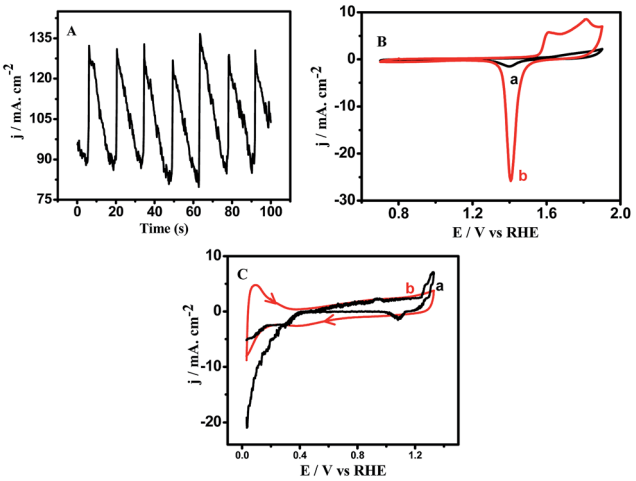

Fig. 1 (A) Chronoamperometric response of gold during anodization; (B) cyclic voltammetric responses (scan rate: 0.05 V s^{-1}) of (a) a bare gold surface; and (b) an electrochemically reduced anodized gold surface; (C) cyclic voltammetric responses (scan rate = 1 V s^{-1}) of anodized gold; and (b) as for but after iridium deposition.

When the anodized gold (without re-reduction, cyclic voltammogram shown in Fig. 1C-a, black) was immersed in a dilute solution of $IrCl_3 \cdot 3H_2O$ (0.01 M) in 0.1 M NaOH (pH 13), a stable thin blue-colored film developed over a period of 5 hours. At the same time, the yellow-colored $IrCl_3$ solution adjacent to the anodized gold surface also turned deep blue. The implication of this observation is that the formation of IrO_x nanoparticles has occurred on the surface (Fig. 1C-b, red) as well as

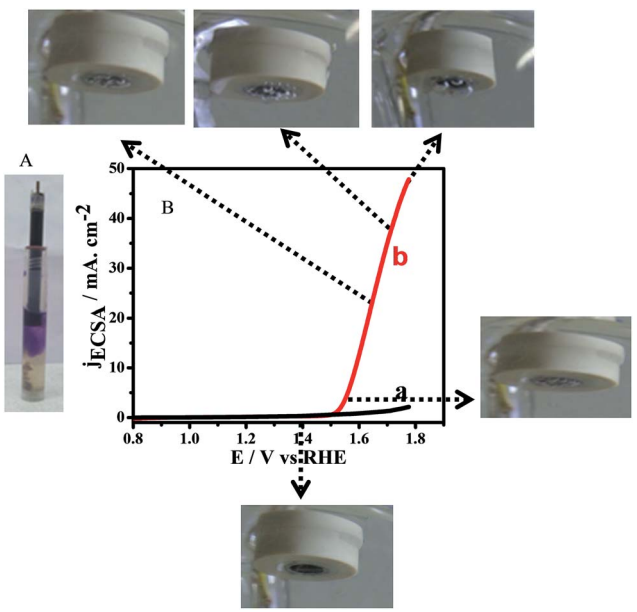

Fig. 2 (A) Photograph showing hexahydroxyiridate(IV) complex formation on the anodized gold electrode surface. (B) Linear sweep voltammetric response obtained at an IrO_x/Au in 0.1 M NaOH with a scan rate of 0.01 V s^{-1}. Photographs of the electrode surface were taken at different applied potentials which show features of the no gas bubbles situation to fully formed bubbles.

in solution (Fig. 2A). The sharp absorption feature at 313 nm confirms the presence of $[Ir(OH)_6]^{2-}$ and the absorption at 581 nm is attributed to the presence of Ir^{IV}–O–Ir^{IV} linkages.[9] Control experiments on the formation of iridium oxide simultaneously acquiring UV-visible spectra and pH data confirmed the formation of hexahydroxyiridate(IV) (Fig. S1–S2†).

Anodized gold is converted to $NaAu(OH)_4$ in strong alkaline (0.1 M NaOH) solutions. The latter is a well-known condensation reagent[16] and on this basis can be expected to cause condensation of $[Ir(OH)_6]^{2-}$. As reported by Zhao *et al.*[9] $IrO_x \cdot nH_2O$ nanoparticle films can be grown anodically on various substrates by electrolyzing $[Ir(OH)_6]^{2-}$ solutions at 1.0 to 1.3 V *vs.* Ag/AgCl. The open circuit potential of anodized gold surface is 1.0 V *vs.* Ag/AgCl [Table S1†] which is adequate to initiate iridium oxide deposition in the alkaline medium by condensation of $[Ir(OH)_6]^{2-}$ without applying any external energy. Iridium oxide deposition is confirmed by showing that reaction of the anodized gold surface with hexahydroxyiridate(IV) formed in 0.1 M NaOH solution yields a deposit of iridium oxide. The reduction of Au^{3+} by Ir^{3+} in basic media was recently taken advantage of in the synthesis of a nanocomposite of dithiolate-appended iridium(IV) complex surrounding the AuNPs, during which Ir^{3+} is oxidized to Ir^{4+}.[17] Similarly in the present case, Ir^{3+} to IrO_x conversion takes place on the anodized gold surface with the surface Au^{3+} converting to AuO_x. In contrast, when the same anodized gold surface is treated with iridium oxide nanoparticles, deposition does not take place (treatment undertaken after violet color formation in the solution). In comparison with the bare gold surface (Fig. S3a†) the deposition of Ir-oxide particles on the anodized gold (Fig. S3b†) can clearly be seen from the FESEM images. A stable and reproducible zeta potential of −35 mV confirms the stability of the particles. EDAX spectra show the presence of Ir (74.4%), oxygen (13.8%), the remainder being Au (11.8%) (Fig. S4†).

Having verified that IrO_x film deposition occurs on the anodized gold, we now turn our attention to its electrochemical characteristics. After IrO_x nanoparticle deposition (Fig. S1B and C†) and as shown in Fig. 1C, well defined hydrogen adsorption–desorption features can be seen along with the disappearance of voltammetric features associated with Au reduction and oxidation features. The broad reversible peak pair at 0.97 V *vs.* RHE with a near-zero peak-to-peak separation (ΔE_p) is indicative of a surface-confined iridium based process.[15] When a pH ~ 7 solution is employed for cycling the potential of the IrO_x/Au over the range of 0.64 V to 1.5 V, two well defined peak pairs at 0.94 V and 1.42 V are discernible (Fig. S5†) which may be assigned to $Ir^{III/IV}$ and $Ir^{IV/V}$ processes.[18] The proximity of $Ir^{III}/Ir^{IV}$and Ir^{V}/Ir^{VI}potentials to the onset of water oxidation suggests that these redox processes are involved in the electrocatalytic water oxidation mechanism. The linear plot of Ir peak currents *vs.* scan rate (Fig. S4†) confirms the presence of surface confined Ir on the Au surface. Fig. S6 and S7† (potential *vs.* pH data) show that the potentials for $Ir^{III/IV}$ and $Ir^{IV/V}$ processes, and the onset potential of O_2 evolution (taken at a current density of 0.5 mA cm^{-2}), all shift by approx. 0.059 V per pH unit. The pH dependence of the Ir based processes implies that they all

involve reversible (Nernstian) coupled one-electron–proton steps that precede the kinetically limited O_2 evolution.

The cyclic voltammograms for the IrO_x/Au electrode obtained over the potential range of 0.4 to 1.3 V (*vs.* Ag/AgCl) as a function of pH (Fig. S5†) show a gradual shift in the onset of oxygen evolution towards less anodic potentials when the potential values are again taken at a current density of 0.5 mA cm^{-2} for comparison with the literature.[19] Another significant feature is that the reversible potential for the $Ir^{IV/V}$ process merges with the OER current onset region as the pH approaches 13. Fig. 2B does not show evidence of gas evolution in the potential region below 1.475 V *vs.* RHE and the electrode starts to evolve gas bubbles at potentials between 1.5 and 1.55 V *vs.* RHE. The OER behaviour of IrO_x/Au is compared with that of polycrystalline iridium (pc-Ir) in both acid and alkaline media (Fig. S6†). In acidic 0.5 M H_2SO_4, there is a negative shift in the OER onset potential of *ca.* 0.040 V for a change from Ir to IrO_x/Au, whereas in alkaline 0.1 M NaOH, a more significant difference is observed in the OER onset potentials (*ca.* 0.076 V) (Fig. S8†). The IrO_x/Au electrode also exhibits a higher water oxidation current at a lower onset potential for oxygen evolution than either the pc-Ir modified or a pc-IrO_x modified electrode in both 0.5 M H_2SO_4 and 0.1 M NaOH.[5]

The chemical nature of IrO_x/Au surface was further confirmed by XPS analysis that reveals the presence of both Ir metal and IrO_x, in a ratio of 59.6 : 40.4 (Fig. 3). A ratio of 57.1 : 42.9 for Au : Au_2O_3 was also obtained, which suggests that part of the anodized Au surface has been reduced back to Au metal, probably by Ir^{3+} (Fig. 3 and S10†). A plausible reaction mechanism is that Ir^{3+} is adsorbed onto the anodized Au surface when the latter is soaked in an alkaline $IrCl_3$ solution. The adsorbed Ir^{3+} then undergoes condensation to form IrO_x on the Au_2O_3 surface which gives the dark brown color, while the Ir^{3+}cation in the solution form a layer close to the electrode surface which reduces Au_2O_3 to Au, with the Ir^{III} cation being oxidized to Ir^{IV}, to give both $[Ir(OH)_6]^{2-}$ and polymerized IrO_x in 0.1 M NaOH (bluish purple in Fig. 2A). The XPS results confirm the observations made in the UV-visible spectral studies presented above. Oxygen gas bubbles are clearly seen by the naked eye when the potential is more positive than ~1.5 V *vs.* RHE (Fig. 2B). The anodized Au surface did not show the corresponding current rise and gas evolution in this potential window confirming that the IrO_x-coated anodized Au surface is responsible for the electrocatalyzed OER. As the surface coverage of IrO_x on the anodized surface is approximately 0.65, one may speculate on the cooperative effect of the oxides of gold and iridium, in addition to the support role played by gold[13] in OER electrocatalysis.

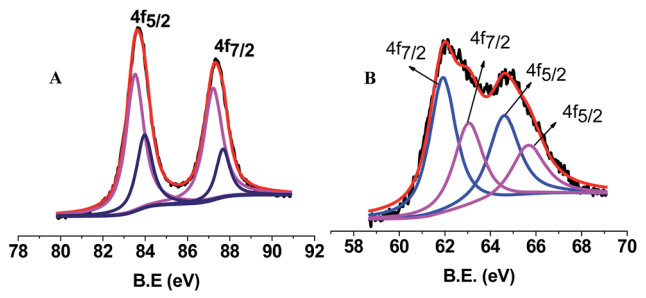

Fig. 3 XPS spectra of Ir and IrO_x deposited on anodized Au surface for (A) Au_2O_3 (rose line); Au (blue line) and (B) IrO_2 (rose line); Ir (blue line).

The present electrocatalytic surface also possesses excellent stability with a sustained current density being maintained for over 120 potential cycles at a scan rate of 0.01 V s^{-1} (Fig. S9†). However, the presence of Ir particles revealed in XPS is surprising. It may be linked to the chemistry of Au nanoclusters (that are likely to arise during the process of AuNPs formation) showing unusual tendency to reduce metal ions.[20] In the present case, although direct experimental evidence is not available at the present time, it may therefore be postulated that the redox chemistry between IrO_x and Au nanoclusters can lead to the formation of zero-valent iridium species.

After establishing the role of anodized gold in facilitating the spontaneous deposition of IrO_x and providing a synergistic support effect in OER electrocatalysis, the catalytic efficiency of this IrO_x/Au electrode was quantified in terms of the turn-over frequency (TOF) value obtained by the analysis of rotating ring-disk electrode voltammetric data (Fig. S11†). The TOF is expressed as the number of moles of O_2 produced per mole of Ir, and is calculated from the oxygen reduction current at the Pt-ring electrode, (i_R), according to the equation

$$\mathrm{TOF} = i_R/N_{CL}\Gamma nAF$$

where n is the number of electrons transferred per oxygen molecule at the Pt-ring electrode ($n = 4$), F is Faraday's constant, A is the area of the disk electrode, Γ is the surface concentration of the catalyst, and N_{CL} is the collection efficiency (refer to ESI† for TOF calculation). The surface concentration of IrO_x was determined from the calculation of the charge associated with the adsorbed hydrogen underpotential deposition process (Fig. 1C) and the charge associated with the $Ir^{IV/V}$ oxidation reaction (Fig. S5†). An average value of ~6.2 s^{-1} was obtained for TOF (at a potential as low as 1.56 V *vs.* RHE) in this study for a surface IrO_x concentration of *ca.* 10^{-9} mol cm^{-2}. In Table S2,† IrO_x/Au is benchmarked against other iridium oxide catalysts. For the sake of an objective evaluation of the activity of IrO_x-electrocatalysts for the water oxidation reaction,[1] it is desirable to have (a) methods of catalyst preparation that are simple and can be standardized easily; and (b) $TOF_{1.56V}$ values on par with those benchmarked[21] (Table S2†). The advantage of the new method is the ease with which this catalytic electrode is prepared that still retains its high OER catalytic efficiency as found with the other more difficult-to-prepare nanoparticulate films. A $TOF_{1.56V}$ value of ~6.2 s^{-1} is close to those reported for other Ir oxide-based catalysts (Table S2†) prepared using more complex methods. The method presented in this work is straightforward and reliable and can have other applications like fabrication of pH-sensitive microelectrodes[22] for example in scanning electrochemical microscopy. To our knowledge, this work provides the first application of anodized gold for the electroless deposition of the iridium oxide catalyst.

Acknowledgements

PEK thanks India's UGC for the award of a senior research fellowship. The authors cherish the experimental work of Late I. Maheshwaran. Financial support from the Australia-India Strategic Research Fund [DST/INT/AUS/P-43/2011] and partial support from [DST: SR/NM/NS-1036/2011] is acknowledged.

References

1 Y. Gorlin and T. F. Jaramillo, *J. Am. Chem. Soc.*, 2010, **132**, 13612.
2 C. C. L. McCrory, S. Jung, J. C. Peters and T. F. Jaramillo, *J. Am. Chem. Soc.*, 2013, **135**, 16977.
3 H. G. Sanchez Casalongue, M. L. Ng, S. Kaya, D. Friebel, H. Ogasawara and A. Nilsson, *Angew. Chem., Int. Ed.*, 2014, **53**, 7169.
4 A. Minguzzi, O. Lugaresi, E. Achilli, C. Locatelli, A. Vertova, P. Ghigna and S. Rondinini, *Chem. Sci.*, 2014, **5**, 3591.
5 H. N. Nong, L. Gan, E. Willinger, D. Teschner and P. Strasser, *Chem. Sci.*, 2014, **5**, 2955.
6 K. E. Michaux and R. W. Murray, *Langmuir*, 2013, **29**, 12254.
7 F. Shao, B. Elias, W. Lu and J. K. Barton, *Inorg. Chem.*, 2007, **46**, 10187.
8 T. Kuwabara, E. Tomita, S. Sakita, D. Hasegawa, K. Sone and M. Yagi, *J. Phys. Chem. C*, 2008, **112**, 3774.
9 Y. Zhao, E. A. Hernadez-Pagan, N. M. Vargas-Barbosa, J. L. Dysart and T. E. Mallouk, *J. Phys. Chem. Lett.*, 2011, **2**, 402.
10 K. Nishio and H. Masuda, *Angew. Chem., Int. Ed.*, 2011, **123**, 1641.
11 W. Zhao, X. Jing-Juan, S. Chuan-Guo and H.-Y. Chen, *Electrochem. Commun.*, 2006, **8**, 773.
12 X. Shili, Y. Yuan, W. Pengshu, Y. Yingchang, X. Yue, L. Jun, L. Zelin and H. Wei, *Int. J. Electrochem. Sci.*, 2013, **8**, 1863.
13 B. S. Yeo and A. T. Bell, *J. Am. Chem. Soc.*, 2011, **133**, 5587.
14 M. Pourbiax, *Atlas of electrochemical equlibria in aqueous solutions*, Pergamon Press, 1st edn, 1966, p. 402.
15 S. Komiya, T. Sone, I. Usui, M. Hirano and A. Fukuoka, *Gold Bull.*, 1996, **29**, 131.
16 G. Nasr, A. Guerlin, F. Dumur, S. A. Baudron, E. Dumas, F. Miomandre, G. Clavier, M. Sliwa and C. R. Mayer, *J. Am. Chem. Soc.*, 2011, **133**, 6501.
17 Y. Zhao, N. M. Vargas-Barbosa, E. A. Hernandez-Pagan and T. E. Mallouk, *Small*, 2011, **7**, 2087.
18 R. D. L. Smith, B. Sporinova, R. D. Fagan, S. Trudel and C. P. Berlinguette, *Chem. Mater.*, 2014, **26**, 1654.
19 O. Diaz-Morales, F. Calle-Vallejo, C. de Munck and M. T. M. Koper, *Chem. Sci.*, 2013, **4**, 2334.
20 P. Rodriguez and M. T. M. Koper, *Phys. Chem. Chem. Phys.*, 2014, **16**, 13583.
21 [Present work]: $\eta = 0.37$ V @10 mA cm^{-2} (in 0.1 M NaOH), [ref. 2]: $\eta = 0.325$ V @10 mA cm^{-2} (in 1 M NaOH).
22 D. O. Wipf and F. Ge, *Anal. Chem.*, 2000, **72**, 4921.